This is the author's final accepted version.

There may be differences between this version and the published version. You are advised to consult the publisher's version if you wish to cite from it.

http://eprints.gla.ac.uk/155380/

Talbot effect for gratings with diagonal symmetry

Jakub Bělín[1, *] and Tomáš Tyc[2, †]

[1]*School of Physics and Astronomy, College of Science and Engineering, University of Glasgow, Glasgow G12 8QQ, UK*
[2]*Department of Theoretical Physics and Astrophysics, Faculty of Science,*
Masaryk University, Kotlářská 2, 61137 Brno, Czech Republic

We show that the phenomenon of self-imaging of infinite periodic gratings, known as Talbot effect, is related not only to the dimensions of an elementary cell of the grating but is also closely connected with its structure. This is demonstrated in a particular class of gratings for which the self-imaging distance differs from the Talbot length as it is usually defined. This phenomenon can be explained by a destructive interference of several fractional Talbot images at the self-imaging distance.

Keywords: Talbot effect, Self-imaging, X-gratings

I. INTRODUCTION

Talbot effect, also referred to as self-imaging or lens-less imaging, is a phenomenon manifested by a periodic repetition of planar field distributions in certain types of wave fields. This phenomenon is finding its applications not only in optics, but also in a variety of research fields, such as acoustics [1], electron microscopy [2], plasmonics [3], X-ray diffraction and imaging [4], non-linear dynamics [5] and Bose-Einstein condensates [6]. In optics, self-imaging is being explored particularly in image processing [7], in the production of spatial-frequency filters [8], photolitography [9] and in optical metrology [10]. The fractal structure of the Talbot effect [11] and its description in a phase-space [12] have also been studied. In this paper, we describe the connection of Talbot effect with the geometry of the grating and show that a special kind of symmetry of certain gratings can lead to a reduction of the Talbot length. Although a similar topic has already been discussed in Ref. [13], our analysis provides a more physical insight. Moreover, derivations included in this work show that the contraction of the self-imaging distance can be explained very easily applying properties of the so-called generalised quadratic Gauss sums, which modulate both the phase and amplitude of the corresponding Talbot image components.

The paper is organized as follows: In Sec. II we recall the definition of Talbot length and it applications to general gratings, in Sec. III we analyze the wave at an arbitrary distance beyond the grating that is a rational multiple of the Talbot length. In Sec. IV we intorduce gratings with a special symmetry which we call X-gratings, and analyze the Talbot length for them. In Sec. V we present our experimental results of Talbot images and conclude in Sec. VI.

---

*Electronic address: j.belin.1@research.gla.ac.uk
†Electronic address: tomtyc@physics.muni.cz

II. TALBOT LENGTH OF A 2D GRATING

In this section we calculate the Talbot length at which self-imaging of a periodic two-dimensional (2D) grating occurs. Consider a rectangular grating with elementary cell basis vectors $\vec{a} = (a, 0, 0)^{\mathrm{T}}, \vec{b} = (0, b, 0)^{\mathrm{T}}$. Let the grating be placed in the plane $z = 0$ and illuminated by monochromatic plane wave with wavelength λ propagating along the z-axis. The complex transmission function of the grating $t(x, y)$ has translational symmetry that can be expressed as

$$t(x, y) = t(x + ma, y + nb), \quad m, n \in \mathbb{N}, \quad (1)$$

which can be expressed as a convolution of the function $t_0(x, y)$ describing one elementary cell of the grating (i.e., $t_0(x, y)$ is nonzero only for $0 \le x < a, 0 \le y < b$) and the two-dimensional Dirac comb:

$$t(x, y) = \iint_{\mathbb{R}^2} t_0(x - \xi, y - \eta) \times$$
$$\times \sum_{m,n=-\infty}^{\infty} \delta(x - ma)\,\delta(y - nb)\,\mathrm{d}\xi\,\mathrm{d}\eta, \quad (2)$$

To propagate this beam, we employ the standard Fourier method: we decompose the initial wave into plane wave components, propagate each of them separately and then compose them again. The Fourier transform $\tilde{t}(k_x, k_y)$ of the wave (2) is

$$\tilde{t}(k_x, k_y) = \frac{(2\pi)^2}{ab}\,\tilde{t}_0(k_x, k_y) \times$$
$$\times \sum_{m,n=-\infty}^{\infty} \delta\left(k_x - m\frac{2\pi}{a}\right)\delta\left(k_y - n\frac{2\pi}{b}\right), \quad (3)$$

where $\tilde{t}_0(k_x, k_y)$ is the Fourier transform of $t_0(x, y)$. This forest of δ-functions corresponds to a grid of bright peaks in the Fourier plane. The transversal part of the wave vector of the (m, n) plane-wave component in Eq. (3) is then $k_\perp = 2\pi\sqrt{m^2/a^2 + n^2/b^2}$ and the corresponding longitudinal component k_z is given, in the paraxial approximation, by

$$k_z = \sqrt{k^2 - k_\perp^2} \approx k - \frac{k_\perp^2}{2k} = k - \pi\lambda\frac{m^2b^2 + n^2a^2}{a^2b^2}, \quad (4)$$

where $k = 2\pi/\lambda$. Now, suppose that the ratio a^2/b^2 is a rational number. This is equivalent to saying that the grating parameters a and b satisfy

$$a^2 = g^2 A, \quad b^2 = g^2 B, \tag{5}$$

where the numbers $A, B \in \mathbb{N}$ are coprime and g is a common factor with the dimension of length. With the help of Eqns. (4) and (5) we can now express the phase of the (m, n) plane-wave component at a distance z beyond the grating as

$$kz - 2\pi \frac{\lambda z}{2g^2 AB} \left(m^2 B + n^2 A\right). \tag{6}$$

The first term is an unimportant global phase that is the same for all the plane-wave components. The second term is the important one. If, for some z, it happens to be an integer multiple of 2π for all m and n, then the wave at that distance z will be the same as the wave at $z = 0$, i.e., immediately beyond the grating. In other words, self-imaging occurs. Since A, B are coprime, this happens when the fraction in Eq. (6) is an integer. The smallest non-zero integer value, unity, then corresponds to the Talbot length [14], for which we get

$$z_{\mathrm{T}} = \frac{2g^2 AB}{\lambda}. \tag{7}$$

This is equal to the smallest common multiple of the Talbot lengths $2g^2 A/\lambda$ and $2g^2 B/\lambda$ of two one-dimensional gratings with grating parameters a and b, respectively.

However, as we will see in the following, in some situations self-imaging may occur even at distances smaller that the Talbot length. To analyse this possibility, in the next section we calculate the diffraction pattern at a rational multiple of the Talbot length.

III. WAVEFUNCTION OF FRACTIONAL TALBOT EFFECT

In this section we will describe the fractional Talbot effect. We will be interested in the diffraction pattern beyond a periodic grating at a rational multiple of the Talbot length, i.e., at the distance

$$z_f = \frac{z_{\mathrm{T}}}{4AB} \frac{P}{Q}, \quad P, Q \in \mathbb{N} \tag{8}$$

To express the wavefunction, it is useful to introduce two pairs of coprime numbers (P_x, Q_x) and (P_y, Q_y) defined by

$$\frac{AP_x}{Q_x} = \frac{BP_y}{Q_y} = \frac{P}{Q}, \tag{9}$$

where the integers A, B are defined by equation (5). By the calculation shown in Appendix we then obtain the

wavefunction in the following form:

$$u(x, y; z_f) = \sum_{m=0}^{2Q_x-1} \sum_{n=0}^{2Q_y-1} t\left(x - a\frac{m}{2Q_x}, y - b\frac{n}{2Q_y}\right) \times$$
$$\times \frac{-\mathrm{i}}{\sqrt{4Q_x Q_y}} S\left(2Q_x, P_x, 2m\right) S\left(2Q_y, P_y, 2n\right), \tag{10}$$

where symbol $S(Q, P, m)$ is defined by the formula

$$S(Q, P, m) = \frac{1}{\sqrt{P}} \sum_{j=0}^{P-1} \exp\left\{\mathrm{i}\pi \frac{Q}{P}\left(j - \frac{m}{2Q}\right)^2\right\} \tag{11}$$

This is an analytical expression of the wavefunction corresponding to the two-dimensional fractional Talbot effect. It tells us that in each plane $z = z_f$ the wave corresponds to a superposition of $4Q_x Q_y$ images of the original grating, spatially shifted in the x and y directions with respect to each other and modulated by the sums $S(2Q_x, P_x, 2m)$ and $S(2Q_y, P_y, 2n)$. Explicit values of these sums can be derived from the properties of generalised quadratic Gauss sums, which have been published in many publications, see e.g. [15]. An important property of the sums $S(Q, P, m)$ arises from these properties, namely if $QP + m$ is an even number [15], they are periodic in both P and m with the period $2Q$, i.e.,

$$S(Q, P, m) = S(Q, P + 2Q, m) = S(Q, P, m + 2Q). \tag{12}$$

Applying this to the sums $S(2Q_x, P_x, 2m)$ and $S(2Q_y, P_y, 2n)$ in Eq. (10), we see that the diffraction pattern is periodic in the z direction—the Talbot effect.

IV. X-GRATINGS

Now we are coming to the key finding of this paper. We will reveal an interesting purely two-dimensional phenomenon connected with one particular type of gratings, which we call **X-gratings** due to the structure of a grating cell which looks like a letter "X". These gratings can in general be described by an arbitrary transmission function $t(x, y)$ with the following property:

$$t(x, y) = t\left(x - \frac{a}{2}, y - \frac{b}{2}\right)$$
$$\neq t\left(x - \frac{a}{2}, y\right) = t\left(x, y - \frac{b}{2}\right) \tag{13}$$

We can interpret this property as follows: if we shift the grating in both the x and y directions by half of the corresponding grating parameter, we will get again the initial pattern. On the other hand, shifting in either x or y direction alone leads to a pattern different from the initial one. At the same time, these two shifts (in either x or y direction) are equivalent. In fact, X-gratings can be regarded to be generalised hexagonal arrays, which occur in nature frequently (honeycomb, graphene, ice etc.)

due to their efficiency: honeycombs require less wax to construct and gain lots of strength under compression. Moreover, many materials with a hexagonal structure are intensively studied [16–20].

As examples of X-gratings, we introduce two patterns: one created by regular triangles and one composed of stars as shown in Fig. 1. Figs. 2 and 3 then illustrate the property (13).
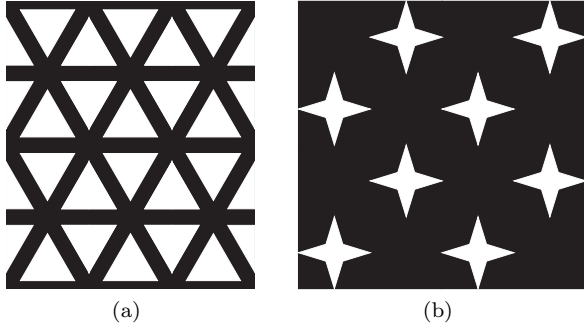
FIG. 1: Examples of X-gratings.
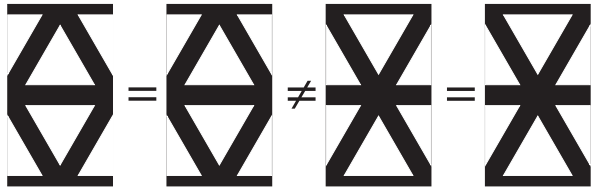
FIG. 2: Example of an X-grating with $|A - B| = 2$. Pictures follow equation (13).

FIG. 3: Example of an X-grating with $|A - B| = 0$. Pictures follow equation (13).

In the particular case shown in Fig. 2, the grating parameters are related to each other as $b = \sqrt{3}a$, and the parameters of Eq. (5) are $A = 1$ and $B = 3$. Therefore the Talbot length, according to equation (7), is equal to

$$z_{\mathrm{T}} = 2\frac{b^2}{\lambda} = 2\frac{3a^2}{\lambda}. \quad (14)$$

Now, let us take a look at the wave function at a distance $z_{\mathrm{T}}/4$. The corresponding parameters are $Q_x = Q_y = Q = 1$, $P_x = P = 3$ and $P_y = 1$. In order to evaluate the wave function at this distance, we need the following values of sums $S(2Q_x, P_x, 2m)$ and $S(2Q_y, P_y, 2n)$:

$$S(2,3,0) = \mathrm{i}, \quad S(2,3,2) = 1,$$
$$S(2,1,0) = 1, \quad S(2,1,2) = \mathrm{i}. \quad (15)$$

From Eq. (10) we then get

$$u\left(x, y; \frac{z_{\mathrm{T}}}{4}\right) = \frac{-\mathrm{i}}{2}[\mathrm{i}t(x,y) + t(x - a/2, y)$$
$$- t(x, y - b/2) + \mathrm{i}t(x - a/2, y - b/2)] = t(x, y), \quad (16)$$

where we have used the property (13). We see a surprising fact—self-imaging occurs already at the distance $z_{\mathrm{SI}} \equiv z_{\mathrm{T}}/4$, i.e., the grating behaves as if it were half-periodic. This is caused by the mutual cancellation of the middle two terms in Eq. (16), or, physically speaking, by destructive interference of the two fractional Talbot images and constructive interference of the other two.

This may also seem strange at first sight because if we insert the distance z_{SI} into the phase (6), the second term will not be equal to an integer multiple of 2π in general, so it is not obvious why self-imaging should be observed. A closer inspection reveals that the structure of an elementary cell of an X-grating causes a modulation of the Fourier image of this grating by a goniometric function such that some bright peaks vanish. The remaining bright peaks then correspond to plane waves which interfere in phase at the distance z_{SI}.

The above discussed result does not hold for all X-gratings, but the shortest self-imaging distance z_{SI} depends on the values of the sums $S(2Q_x, P_x, 2m)$ and $S(2Q_y, P_y, 2n)$. To specify it, it is natural to assume that z_{SI} corresponds to the minimal possible values of parameters Q_x and Q_y (since the wave is a superposition of $4Q_xQ_y$ images of the original grating). Therefore we set $Q_x = Q_y = 1$ at the distance z_{SI}. The parameter Q in Eq. (9) must then be equal to unity as well because P and Q are coprime. Equation (9) also yields $AP_x = BP_y$; from the fact that A and B are coprime it then follows that $P_x = NB$ and $P_y = NA$, where N is a natural number. Finally, the distance z_{SI} can be obtained from Eq. (8) (with $Q = 1$ and $P = AP_x = BP_y = NAB$) as

$$z_{\mathrm{SI}} = N\frac{z_{\mathrm{T}}}{4}. \quad (17)$$

The number N could be estimated from explicit values of sums $S(2, NB, 2m)$ and $S(2, NA, 2n)$. This analysis reveals that the ratio $z_{\mathrm{SI}}/z_{\mathrm{T}}$ is determined by the value of $|A - B|$ mod 4 due to the periodicity of S [since $S(2, P, 2m) = S(2, P + 4, 2m)$]. However, in the following we provide a simpler way of finding the self-imaging distance z_{SI} by employing geometrical and physical arguments. We discuss the four possibilities for $|A - B|$ mod 4 separately:

- $|A - B|$ mod $4 = 0$: according to Eq. (10), an exact image of the grating but shifted by a half of the grating parameter in both x and y directions is created at a half of the Talbot length. However, according to condition (13) the image shifted in this way is exactly the same as an unshifted one, so $z_{\mathrm{SI}} = z_{\mathrm{T}}/2$ and therefore $N = 2$ in Eq. (17). In the specific case of $A = B$, it is possible to choose

another orthogonal basis $(\vec{a}', \vec{b}')$ for these gratings, rotated by angle $\pi/4$ with respect to the original basis $(\vec{a}, \vec{b})$. By doing this, we realise that $a' = b' = a/\sqrt{2}$ and z_T is equal to the Talbot distance calculated from the new grating periods a' and b'. This is the case of the grating shown in Fig. 1 (b).

- $|A - B| \bmod 4$ is either 1 or 3: then either A or B is an even number and the second one is odd number. As we have mentioned, the Talbot length for two-dimensional grating corresponds to the smallest common multiple of Talbot lengths of the two corresponding 1D gratings oriented in the x and y directions. This means that in half of the Talbot length we obtain an image shifted by $aA/2$ in x-direction and by $bB/2$ in y-direction, but since one of the parameters A, B is an even number, we get (applying periodicity) an unshifted image in one direction and shifted image in the second one. Therefore in this case $z_\mathrm{SI} = z_\mathrm{T}$ and $N = 4$ in Eq. (17).

- $|A - B| \bmod 4 = 2$: this is the most interesting case. To find the wavefunction at the distance $z_T/4$, the sums $S(2, B, 0)$, $S(2, B, 2)$, $S(2, A, 0)$ and $S(2, A, 2)$ must be evaluated. The case of $A = 3$ and $B = 1$ was discussed earlier and we showed that self-imaging can be observed at distance $z_T/4$. One can show that this is a general result for all gratings with $|A - B| \bmod 4 = 2$ by realising that the sums $S(2, P, m)$ are periodic in P with a period 4 and therefore sums $S(2, P, m) = S(2, P \bmod 4, m)$. For this reason we can substitute $A \bmod 4$ and $B \bmod 4$ instead of A and B, respectively, into the above sums. But A and B are coprime, which, together with the condition $|A - B| \bmod 4 = 2$, implies that they are both odd numbers. There are only two possible values, 1 and 3, for the remainder after dividing an odd number by 4. This reduces the situation to the above discussed special case of $A = 3$ and $B = 1$ and the self-imaging distance is therefore $z_\mathrm{SI} = z_T/4$ and therefore $N = 1$ in Eq. (17).

The ratio $z_\mathrm{SI}/z_\mathrm{T}$ toghether with corresponding value of parameter N (defined in Eq. (17)) is summarised in Table I, which is the main result of this paper.

TABLE I: Self-Imaging distances for X-gratings

$|A - B| \bmod 4$	N	$z_\mathrm{SI}/z_\mathrm{T}$
0	2	1/2
1	4	1
2	1	1/4
3	4	1

Gratings with hexagonal symmetry have $b = \sqrt{3}a$, $A = 1$ and $B = 3$ and therefore they belong to the most interesting category of $|A - B| \bmod 4 = 2$. One example is
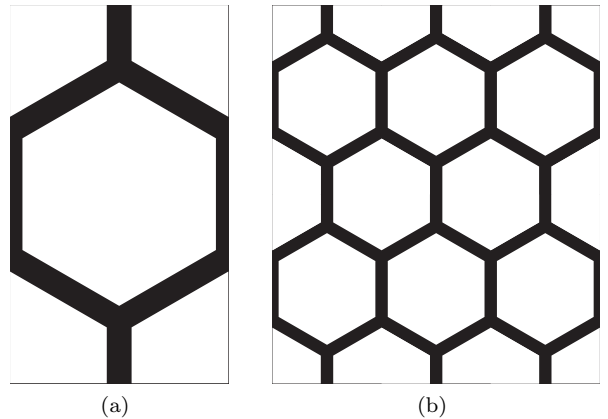
FIG. 4: Another example of X-grating with hexagonal symmetry: (a) Its elementary cell and (b) a larger section.

the grating of Figs. 1(a) and 2, another example is shown in Fig. 4. The self-imaging distance is then $z_\mathrm{SI} = z_\mathrm{T}/4$.

Interestingly, the same results could be obtained by choosing a non-orthogonal basis of the grating vectors as shown in the paper of Winthrop and Worthington [13]. They derived a formula defining the distances q of all possible self-imaging two-dimensional arrays

$$q = \frac{\nu a' b' R_a R_b M \sin^2 \gamma}{\lambda}, \qquad (18)$$

where ν, M are integers, a', b' are lengths of the new lattice vectors, γ is the angle between them, and R_a, R_b are integers with no common factor chosen such that $R_a a' = R_b b'$. For example, considering X-grating shown in Fig. 4, using $a' = a$, $b' = a$, $\nu = 1$, $M = 1$, $R_a = 1$, $R_b = 1$, $\gamma = \pi/3$, we arrive at $q = z_\mathrm{SI}$, which confirms our result. At the same time, our computations provide new, more geometric and physical view on the relationship between the self-imaging distance and the symmetry of grating expressed by equation (13).

V. EXPERIMENT

We have also verified our theoretical predictions experimentally. An unpolarised diode laser beam of $\lambda = 532$ nm was focused by an aspherical lens onto one end of a single-mode optical fibre, and the light exiting the other end (having been spatialy filtered by the fibre this way) was collimated by a plano-convex lens of $f = 500$ mm. The grating was placed immediately behind the lens and the diffraction pattern was recorded by a CMOS camera (without objective lens) at a variable distance z behind the grating.

We tested the agreement between theory and experiment on two X-gratings with hexagonal symmetry described in the previous section. These gratings have been manufactured by direct laser lithography; the pattern is

written in a thin chromium layer which has been deposited on a 2 mm thick glass substrate of area $4 \times 4\,\mathrm{cm}^2$. The first grating consisted of regular hexagons arranged in a frame with six-fold symmetry (Fig. 4). The sides of the transparent part had a length 0.45 mm and the edges between two hexagons were 0.1 mm thick. The corresponding parameters were $a = 0.88$ mm, $b = 1.52$ mm and the Talbot length was $z_\mathrm{T} \doteq 8734$ mm. The self-imaging distance then was $z_\mathrm{SI} = z_\mathrm{T}/4 \doteq 2184$ mm.

The second grating consisted of regular triangles arranged in a frame with six-fold symmetry (Figs. 1(a) and 2). The sides of the triangles had the length of 0.654 mm and the bars between neighbouring triangles were 0.2 mm thick. The corresponding parameters were $a = 1$ mm, $b = 1.73$ mm and the Talbot length was $z_\mathrm{T} \doteq 11278$ mm. The self-imaging distance then was $z_\mathrm{SI} = z_\mathrm{T}/4 \doteq 2820$ mm.

The experimental results are presented in Figs. 5, 6 and 7. Fig. 5 shows experimentally obtained Talbot images of gratings 4 and 1(a) at distance $z = z_\mathrm{SI}$, Figs. 6 and 7 are presented alongside with the theoretically predicted Talbot images for several distances from the gratings. Theoretically predicted Talbot images have been computed in MATLAB with a sufficient resolution by combining the multiple shifted images using Eq. (10).

Although the experimentally obtained images are very similar to the theoretically predicted ones, we see some additional irregular streaky patterns in the experimental results. These reflect the difference between our theoretical assumptions and the experimental reality. Our analysis included the paraxial approximation as well as the assumptions about the grating extending to infinity and about unlimited spatial frequencies. These conditions are satisfied only approximately in a real experiment. (Some effects related to spatial frequency limitations have been discussed in ref. [11].) Moreover, our gratings were deposited on a normal glass substrate, so there are slight random phase variations across them; this is probably the most important reason for the imperfections in the experimental results.

VI. CONCLUSION

We have analysed Talbot effect for gratings with a special symmetry properties, the so-called X-gratings. We have shown that the self-imaging distance in general differs from the Talbot distance calculated based on the basis orthogonal grating vectors. This feature can be understood by a destructive interference between two copies of the shifted gratings originating from the fractional Talbot effect, and constuctive interference between the two unshifted ones. This demonstrates that the symmetry of the grating elementary cell has a strong influence on the optical properties and can lead to unexpected interesting phenomena. Although the self-imaging distance z_SI can also be obtained by using a non-orthogonal grating vectors [13], our approach based on geometrical properties of
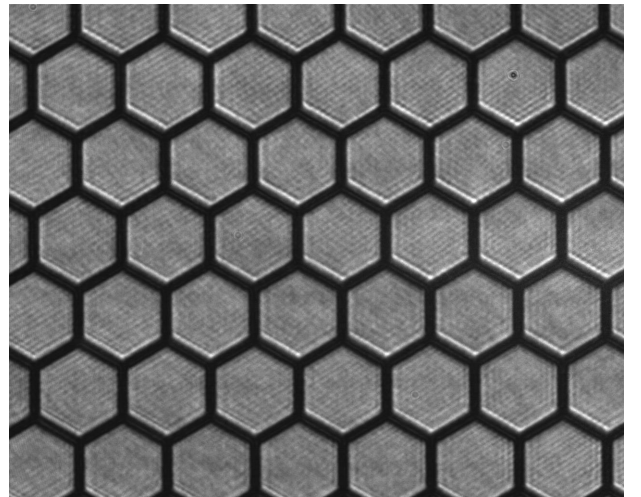
(a) $z = 2190$ mm $\doteq z_\mathrm{SI}$
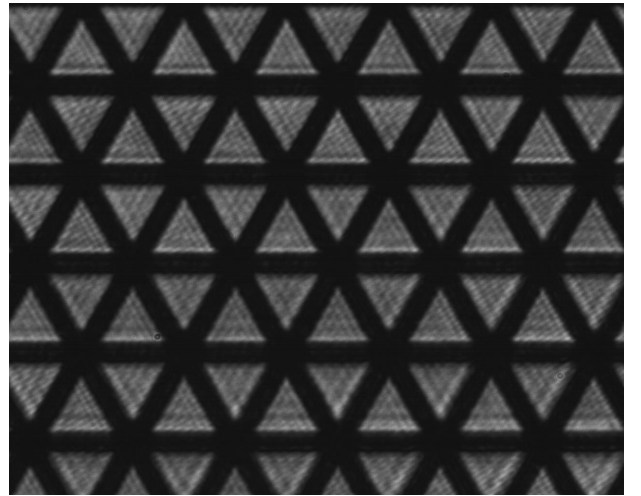
(b) $z = 2830$ mm $\doteq z_\mathrm{SI}$

FIG. 5: Experimental results for X-gratings composed of a) regular hexagons and b) regular triangles obtained at distance $z \doteq z_\mathrm{SI} = z_\mathrm{T}/4$. These results are in a good agreement with our theoretical prediction.

lattice cells and generalised quadratic Gauss sums reveals how the symmetry of the grating leads to reduction of the self-imaging distance. Finally, we have demonstrated the theoretically described phenomena experimentally, finding a good agreement.

(a) Experiment; $z = 729$ mm $\doteq \frac{1}{3} z_{\mathrm{SI}}$

(b) Theory; $z = \frac{1}{3} z_{\mathrm{SI}}$

(c) Experiment; $z = 162$ mm $\doteq \frac{2}{27} z_{\mathrm{SI}}$

(d) Theory; $z = \frac{2}{27} z_{\mathrm{SI}}$
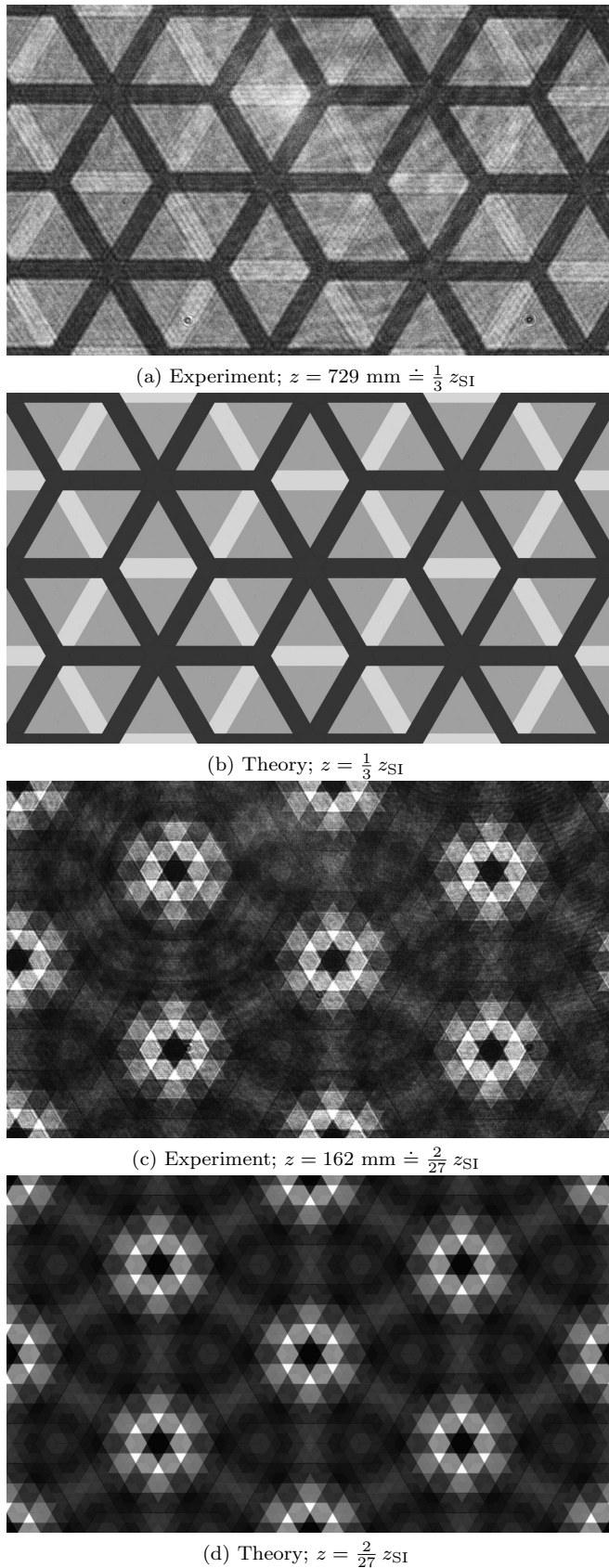
FIG. 6: Comparison of observed and theoretically predicted Talbot images at several distances from the grating composed of regular hexagons. It is obvious that the observed images correspond to those numerically computed very well.

(a) Experiment; $z = 939$ mm $\doteq \frac{1}{3} z_{\mathrm{SI}}$

(b) Theory; $z = \frac{1}{3} z_{\mathrm{SI}}$

(c) Experiment; $z = 162$ mm $\doteq \frac{1}{13} z_{\mathrm{SI}}$

(d) Theory; $z = \frac{1}{13} z_{\mathrm{SI}}$
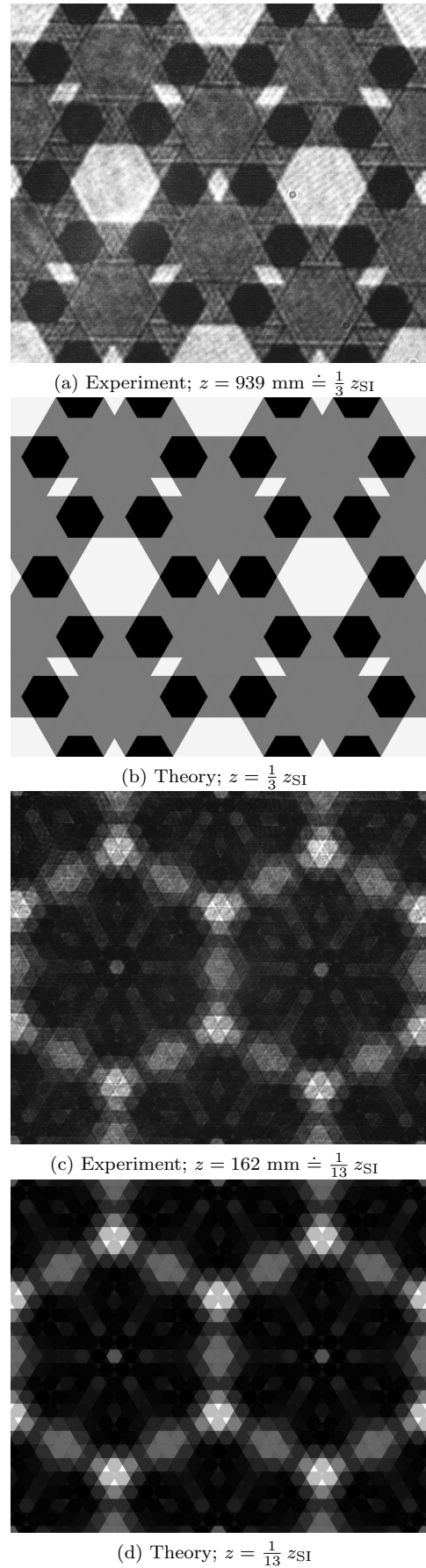
FIG. 7: Comparison of observed and theoretically predicted Talbot images in several distances from the grating composed of regular triangles. As in the previous cases, experimentally obtained and numerically computed images are almost indistinguishable.

Appendix: Fractional Talbot effect

Now we will describe the wavefunction in any rational fraction of the Talbot length: the *fractional Talbot effect*. Just for the sake of clarity, we make the computation for one-dimensional case (generalisation for two-dimensional one is straightforward). Let a one-dimensional infinite periodic grating be described by the complex transmission function $t(\xi)$. If we assume a plane-wave illumination, one can determine the wave $u(x; z)$ by a convolution of the grating function and one-dimanesional Fresnel propagator [21]

$$F_{1D}(x; z) = \frac{\mathrm{e}^{-\mathrm{i}\frac{\pi}{4}}}{\sqrt{\lambda z}} \mathrm{e}^{\mathrm{i}\frac{k}{2z}x^2}. \tag{19}$$

Note that this propagator corresponds to a paraxial approximation of a cylindrical wave. Considering this propagator, we get the following expression for the wavefunction:

$$u(x; z) = \frac{\mathrm{e}^{-\mathrm{i}\frac{\pi}{4}}}{\sqrt{\lambda z}} \int_{\mathbb{R}} t(\xi)\mathrm{e}^{\mathrm{i}\frac{k}{2z}(x-\xi)^2}\mathrm{d}\xi. \tag{20}$$

The grating function $t(\xi)$ can be expressed as another convolution of function of one grating cell $t_0(\xi')$, which is defined on the interval $[-\frac{a}{2}; \frac{a}{2}]$, and the Dirac comb, which periodically replicates the single cell:

$$t(\xi) = [t_0 * D](\xi) = \sum_{m=-\infty}^{\infty} \int_{-\frac{a}{2}}^{\frac{a}{2}} t_0(\xi')\delta(\xi - \xi' - ma)\,\mathrm{d}\xi'. \tag{21}$$

If we insert this result to the integral (20) and exchange the order of summation and integrations, we get a formula in which integral over the size of one single cell occurs:

$$u(x; z) = \frac{\mathrm{e}^{-\mathrm{i}\frac{\pi}{4}}}{\sqrt{\lambda z}} \sum_{m=-\infty}^{\infty} \int_{-\frac{a}{2}}^{\frac{a}{2}} \mathrm{d}\xi'\, t_0(\xi')\times$$
$$\times \int_{\mathbb{R}} \mathrm{d}\xi\, \delta(\xi - \xi' - ma)\, \mathrm{e}^{\mathrm{i}\frac{k}{2z}(x-\xi)^2} =$$
$$= \frac{\mathrm{e}^{-\mathrm{i}\frac{\pi}{4}}}{\sqrt{\lambda z}} \int_{-\frac{a}{2}}^{\frac{a}{2}} \mathrm{d}\xi'\, t_0(\xi') \sum_{m=-\infty}^{\infty} \mathrm{e}^{\mathrm{i}\frac{ka^2}{2z}\left(\frac{x-\xi'}{a}-m\right)^2}. \tag{22}$$

To solve this integral, we need to evaluate the sum in equation (22). Let us choose the distance z such that the fraction $ka^2/2z$ is a rational number multiplied by 2π (the reason of this choice arises from following computations):

$$\frac{ka^2}{2z} = \frac{Q}{P}2\pi \quad \Rightarrow \quad z = \frac{a^2}{\lambda}\frac{P}{2Q} = z_\mathrm{T}\frac{P}{4Q}, \qquad P, Q \in \mathbb{N} \tag{23}$$

For simplicity, numbers P, Q can be considered to be coprime. Inserting this expression to the sum in equation (22) we obtain the following sum:

$$\sum_{m=-\infty}^{\infty} \mathrm{e}^{\mathrm{i}2\pi\frac{Q}{P}\left(\frac{x-\xi'}{a}-m\right)^2} = \mathrm{e}^{\mathrm{i}2\pi\frac{Q}{P}\left(\frac{x-\xi'}{a}\right)^2}\times$$
$$\times \sum_{m=-\infty}^{\infty} \mathrm{e}^{\mathrm{i}2\pi\frac{Q}{P}\left(m^2-2\frac{x-\xi'}{a}m\right)}. \tag{24}$$

The sum on the right-hand side in equation (24) can be rewritten in terms of P sums given by remainders after division of m by number P, i.e. $m = lP + j$.

It is obvious that indices l and j have become new summation indices. Using the identity $\mathrm{e}^{\mathrm{i}2\pi QPl^2} = \mathrm{e}^{\mathrm{i}2\pi Q2l} = 1$ we obtain an important intermediate result:

$$\mathrm{e}^{\mathrm{i}2\pi\frac{Q}{P}\left(\frac{x-\xi'}{a}\right)^2} \sum_{m=-\infty}^{\infty} \mathrm{e}^{\mathrm{i}2\pi\frac{Q}{P}\left(m^2-2\frac{x-\xi'}{a}m\right)}$$
$$= \sum_{j=0}^{P-1} \mathrm{e}^{\mathrm{i}2\pi\frac{Q}{P}\left(j-\frac{x-\xi'}{a}\right)^2} \sum_{l=-\infty}^{\infty} \mathrm{e}^{-\mathrm{i}4\pi Ql\frac{x-\xi'}{a}} =$$
$$= \sum_{j=0}^{P-1} \mathrm{e}^{\mathrm{i}2\pi\frac{Q}{P}\left(j-\frac{x-\xi'}{a}\right)^2} \left(\frac{a}{2Q}\right) \sum_{n=-\infty}^{\infty} \delta\left(x - \xi' - n\frac{a}{2Q}\right). \tag{25}$$

The last step remains: insert this formula to the equation (22). The infinite sum of delta-distributions turns into a finite sum after integration, because only $2Q$ terms of the sum actually lie in the interval $[-\frac{a}{2}; \frac{a}{2}]$. However, the argument of the delta-function in equation (25) should not exceed the range where the elementary cell is defined. Therefore, we introduce a shift $x \to x - n_0 a$ such that the argument of the delta function is in range $[-\frac{a}{2}; \frac{a}{2}]$ for all $2Q$ terms of the sum. Applying this procedure and defining the sum $S(2Q, P, 2n)$ as

$$S(2Q, P, 2n) \equiv \frac{1}{\sqrt{P}} \sum_{j=0}^{P-1} \mathrm{e}^{\mathrm{i}2\pi\frac{Q}{P}\left(j-\frac{n}{2Q}\right)^2} \tag{26}$$

we get

$$u\left(x; z_\mathrm{T}\frac{P}{4Q}\right) = \frac{\mathrm{e}^{-\mathrm{i}\frac{\pi}{4}}}{\sqrt{2Q}} \sum_{n=0}^{2Q-1} t_0\left(x - n_0 a - a\frac{n}{2Q}\right)\times$$
$$\times S(2Q, P, 2n). \tag{27}$$

This expression can be simplified if function of one elementary cell $t_0(x)$ is replaced by the grating function $t(x)$. By doing this, the final result is obtained:

$$u\left(x; z_\mathrm{T}\frac{P}{4Q}\right) = \frac{\mathrm{e}^{-\mathrm{i}\frac{\pi}{4}}}{\sqrt{2Q}} \sum_{n=0}^{2Q-1} t\left(x - a\frac{n}{2Q}\right) S(2Q, P, 2n). \tag{28}$$

This equation describes a wavefunction corresponding to the one-dimensional fractional Talbot effect. Two-dimensional generalization of this formula can be achieved analogously and the result corresponds to equation (10).

[1] Noriaki Saiga and Yoshiki Ichioka. Visualization of the strain wave front of a progressive acoustic wave based on the Talbot effect. *Applied optics*, 24(10):1459–1465, 1985.

[2] Benjamin J McMorran and Alexander D Cronin. An electron Talbot interferometer. *New Journal of Physics*, 11(3):033021, 2009.

[3] Mark R. Dennis, Nikolay I. Zheludev, and F. Javier García de Abajo. The plasmon Talbot effect. *Opt. Express*, 15(15):9692–9700, Jul 2007.

[4] Franz Pfeiffer, Timm Weitkamp, Oliver Bunk, and Christian David. Phase retrieval and differential phase-contrast imaging with low-brilliance X-ray sources. *Nature physics*, 2(4):258–261, 2006.

[5] Yong Zhang, Jianming Wen, S. N. Zhu, and Min Xiao. Nonlinear Talbot Effect. *Phys. Rev. Lett.*, 104:183901, May 2010.

[6] Krzysztof Gawryluk, Mirosaw Brewczyk, Mariusz Gajda, and Jan Mostowski. Formation of soliton trains in BoseEinstein condensates by temporal Talbot effect. *Journal of Physics B: Atomic, Molecular and Optical Physics*, 39(1):L1, 2006.

[7] Albert Wang, Patrick Gill, and Alyosha Molnar. Light field image sensors based on the Talbot effect. *Applied optics*, 48(31):5897–5905, 2009.

[8] AW Lohmann, J Ojeda-Castañeda, and EE Sicre. Multiple interaction bandstop filters based on the Talbot effect. *Optics communications*, 49(6):388–392, 1984.

[9] Michael S Chapman, Christopher R Ekstrom, Troy D Hammond, Jörg Schmiedmayer, Bridget E Tannian, Stefan Wehinger, and David E Pritchard. Near-field imaging of atom diffraction gratings: The atomic Talbot effect. *Physical Review A*, 51(1):R14, 1995.

[10] G Schirripa Spagnolo, D Ambrosini, and D Paoletti. Displacement measurement using the Talbot effect with a Ronchi grating. *Journal of Optics A: Pure and Applied Optics*, 4(6):S376, 2002.

[11] Michael Victor Berry and Sz Klein. Integer, fractional and fractal Talbot effects. *Journal of modern optics*, 43(10):2139–2164, 1996.

[12] Konrad Banaszek, Krzysztof Wódkiewicz, and Wolfgang Peter Schleich. Fractional Talbot effect in phase space: A compact summation formula. *Optics express*, 2(5):169–172, 1998.

[13] John T Winthrop and C Roy Worthington. Theory of Fresnel images. I. Plane periodic objects in monochromatic light. *JOSA*, 55(4):373–381, 1965.

[14] Johannes Courtial, Graeme Whyte, Zdeniek Bouchal, and Jaroslav Wagner. Iterative algorithms for holographic shaping of non-diffracting and self-imaging light beams. *Optics express*, 14(6):2108–2116, 2006.

[15] JH Hannay and Michael V Berry. Quantization of linear maps on a torus-Fresnel diffraction by a periodic grating. *Physica D: Nonlinear Phenomena*, 1(3):267–290, 1980.

[16] Jamie H Warner, Mark H Rümmeli, Ling Ge, Thomas Gemming, Barbara Montanari, Nicholas M Harrison, Bernd Büchner, and G Andrew D Briggs. Structural transformations in graphene studied with high spatial and temporal resolution. *Nature nanotechnology*, 4(8):500–504, 2009.

[17] Ahmad Umar and YB Hahn. Zno nanosheet networks and hexagonal nanodiscs grown on silicon substrate: growth mechanism and structural and optical properties. *Nanotechnology*, 17(9):2174, 2006.

[18] Subhajit Biswas and Soumitra Kar. Fabrication of ZnS nanoparticles and nanorods with cubic and hexagonal crystal structures: a simple solvothermal approach. *Nanotechnology*, 19(4):045710, 2008.

[19] Karl Börjesson, Erik P Lundberg, Jakob G Woller, Bengt Nordén, and Bo Albinsson. Soft-Surface DNA Nanotechnology: DNA Constructs Anchored and Aligned to Lipid Membrane. *Angewandte Chemie International Edition*, 50(36):8312–8315, 2011.

[20] Li Song, Lijie Ci, Hao Lu, Pavel B Sorokin, Chuanhong Jin, Jie Ni, Alexander G Kvashnin, Dmitry G Kvashnin, Jun Lou, Boris I Yakobson, et al. Large scale growth and characterization of atomic hexagonal boron nitride layers. *Nano letters*, 10(8):3209–3215, 2010.

[21] M. Born, E. Wolf, and A.B. Bhatia. *Principles of Optics: Electromagnetic Theory of Propagation, Interference and Diffraction of Light*. Cambridge University Press, 1999.